



Characterizing the attenuation of coaxial and rectangular microwave-frequency waveguides at cryogenic temperatures

Philipp Kurpiers* , Theodore Walter, Paul Magnard, Yves Salathe and Andreas Wallraff

*Correspondence:
philipp.kurpiers@phys.ethz.ch
Department of Physics, ETH Zürich,
Zürich, CH-8093, Switzerland

Abstract

Low-loss waveguides are required for quantum communication at distances beyond the chip-scale for any low-temperature solid-state implementation of quantum information processors. We measure and analyze the attenuation constant of commercially available microwave-frequency waveguides down to millikelvin temperatures and single photon levels. More specifically, we characterize the frequency-dependent loss of a range of coaxial and rectangular microwave waveguides down to 0.005 dB/m using a resonant-cavity technique. We study the loss tangent and relative permittivity of commonly used dielectric waveguide materials by measurements of the internal quality factors and their comparison with established loss models. The results of our characterization are relevant for accurately predicting the signal levels at the input of cryogenic devices, for reducing the loss in any detection chain, and for estimating the heat load induced by signal dissipation in cryogenic systems.

1 Introduction

Interconverting the quantum information stored in stationary qubits to photons and faithfully transmitting them are two basic requirements of any physical implementation of quantum computation [1]. Coherent interaction of solid-state and atomic quantum devices with microwave photons has been experimentally demonstrated for quantum dot systems [2–5], individual electron spin qubits [6], ensembles of electronic spins [7], superconducting circuits [8–10] and Rydberg atoms [11–14].

In the field of circuit quantum electrodynamics, experiments show the ability to use single itinerant microwave photons [15, 16] or joint measurements [17] to generate entanglement between distant superconducting qubits [18]. In these probabilistic entanglement schemes the entanglement generation rate is inversely proportional to the signal loss between the two sites. Furthermore, entanglement can be generated deterministically by transmitting single microwave photons with symmetric temporal shape [19] which can be emitted [20, 21] and reabsorbed with high fidelity [22]. However, the fidelity of the entangled state is dependent on the signal loss for most protocols. Therefore, the ability to transmit microwave photons with low loss, which we address in this manuscript, is essential for the realization of quantum computation with solid-state and atomic quantum systems.

Table 1 Summary of waveguide and measurement parameters

ID	CC085NbTi	CC085Nb	CC141Al	CC085Cu	WR90Alc	WR90Al	WR90CuSn
dim. [mm (in)]	2.2 (0.085)	2.2 (0.085)	3.6 (0.141)	2.2 (0.085)	WR90	WR90	WR90
conductor	NbTi/NbTi	Nb/Nb	Al/SPC	Cu/SPCW	coated Al	Al	Cu-Sn
dielectric	ldPTFE	ldPTFE	ldPTFE	sPTFE	vacuum	vacuum	vacuum
length [mm (in)]	110	110	900	120	304.8 (12)	304.8 (12)	304.8 (12)
T (BT) [mK]	120	50	60	15	60	25	50
T (4K) [K]	4.0	4.0	4.0	4.1	4.3	4.0	4.0
ν range [GHz]	4.2-12.7	4.1-12.5	3.5-12.7	3.6-12.7	7.9-12.3	7.7-12.8	7.7-12.8
\bar{n} (BT)	0.1-2	0.3-10	1-2	1-3	0.2-1	1-4	1-3
\bar{n} (4K)	0.4-5	0.2-4	8-16	4-9	2-10	3-12	5-20

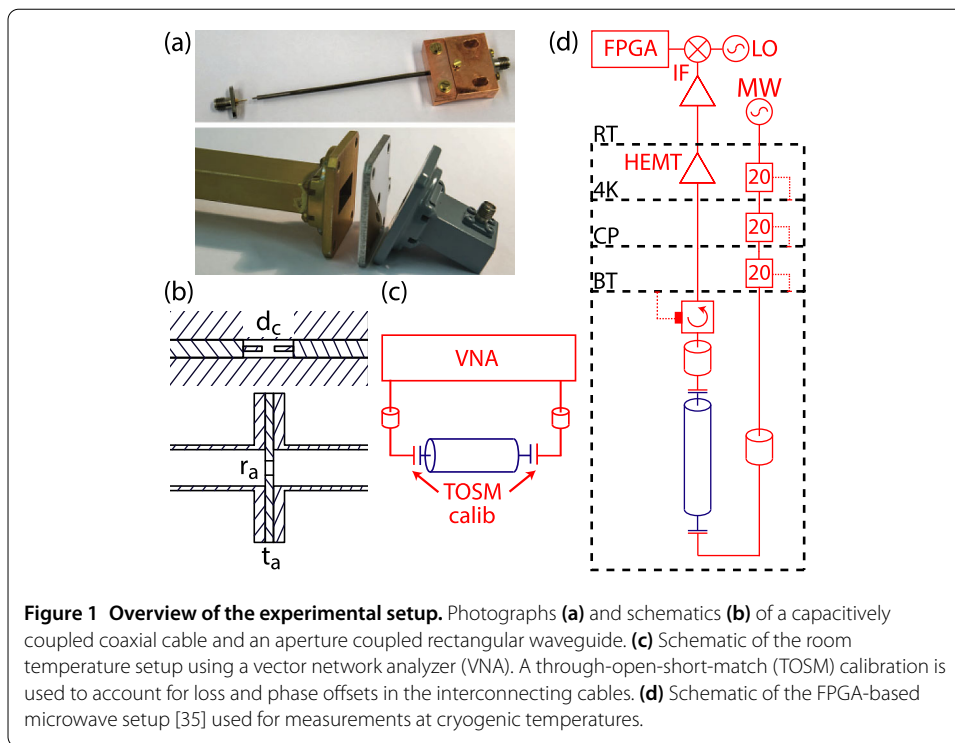
The indicated dimension (dim.) specifies the outer diameter of the coaxial cables and the EIA type of the rectangular waveguides. The conductor and dielectric materials are specified as well as the length of the resonant section employed for the measurements. The temperature T measured at the waveguide is indicated. The average photon number on resonance is shown for the investigated frequency (ν) range.

In addition, studying the reduction of loss of superconducting waveguides has the potential to contribute to improving the fidelity of qubit state measurements [1] by minimizing the loss of the signal between the read-out circuit and the first amplifier [23]. Knowing the loss of microwave waveguides also enables more accurate estimates of the signal levels at the input of cryogenic devices and could be used to better evaluate the heat load induced by signal dissipation.

Previous studies of the attenuation constant were performed for different types of superconducting coaxial cables down to 4 K by impedance matched measurements [24–31]. In those works, the attenuation constant is typically evaluated from measurements of the transmission spectrum of the waveguide, which is subsequently corrected for the attenuation in the interconnecting cables from room temperature to the cold stage in a reference measurement. In these studies lengths of the low-loss superconducting waveguides between 20 m and 400 m were used for the measurements to be dominated by the device under test.

In this paper, we study the loss of coaxial cables and rectangular waveguides using a resonant-cavity technique from which we extract attenuation constants down to 0.005 dB/m accurately between room and cryogenic temperatures at the tens of millikelvin level. By utilizing higher-order modes of these resonators we measure the frequency dependence of the attenuation for a frequency range between 3.5 and 12.8 GHz at cryogenic temperatures only limited by the bandwidth of our detection chain. By comparing our data to loss models capturing this frequency range we extract the loss tangent and relative permittivity of the dielectric and an effective parameter characterizing the conductor loss.

We evaluate the attenuation constant of coaxial and rectangular waveguides made by a number of different manufacturers from a range of materials, see Table 1. We characterize 2.2 mm (0.085 in) diameter coaxial cables with niobium-titanium (Nb-47 weight percent (wt%) Ti) or niobium outer and center conductors. For both cables the manufacturer Keycom Corporation [32] used a low density polytetrafluorethylen (ldPTFE) dielectric. We also measure an aluminum outer, silver plated copper wire (SPC)^a center conductor coaxial cable with an ldPTFE dielectric and an outer diameter of 3.6 mm (0.141 in) manufactured by Micro-Coax, Inc. [33]. As a reference, we analyze a standard copper outer, silver plated copper clad steel (SPCW)^b center conductor coaxial cable with a solid PTFE (sPTFE) dielectric and an outer conductor diameter of 2.2 mm (0.085 in) manu-



factured by Micro-Coax, Inc. [33]. We investigate rectangular waveguides of type WR90 by Electronic Industries Alliance (EIA) standard with inner dimensions of $s_1 = 22.86$ mm, $s_2 = 10.16$ mm ($s_1 = 0.900$ in, $s_2 = 0.400$ in) with a recommended frequency band of 8.2 to 12.4 GHz. Three different conductor materials are characterized: aluminum 6061 with chromate conversion coating per MIL-C-5541E, aluminum 6061 without further surface treatment and oxygen-free, high conductivity (OFHC) copper with tin (Sn wt% > 99.99%) plating of thickness 5-10 μm on the inner surface. All three rectangular waveguides are manufactured by Penn Engineering Components, Inc. [34].

2 Experimental setup

We construct resonators from coaxial cables and rectangular waveguides as shown in the photographs and schematics of Figure 1(a) and (b). For the coaxial cables we use sub-miniature version A (SMA) panel mount connectors and remove the outer conductor and dielectric material of the coaxial cable at both ends to realize a capacitive coupling between the center conductor of the cable and the connector. We choose a coupling capacitance to obtain largely undercoupled resonators (see Section 3 and Appendix 1 for details).

At room temperature (RT) we use a vector network analyzer (VNA) and a through-open-short-match (TOSM) calibration to set the measurement reference plane to the input of the coupling ports of the waveguide according to the schematic presented in Figure 1(c) and adjust the input and output coupling to be approximately equal. For measurements at cryogenic temperatures the microwave signal propagates through a chain of attenuators of 20 dB each at the 4 K, the cold plate and the base temperature stages before entering the waveguide (Figure 1(d)). The output signal is routed through an isolator with a frequency range of 4-12 GHz and an isolation larger than 20 dB, a high-electron-mobility transistor (HEMT) amplifier with a bandwidth of 1-12 GHz, a gain of 40 dB and a noise

temperature of 5 K, as specified by the manufacturer. After room temperature amplification and demodulation, the signal is digitized and the amplitude is averaged using a field programmable gate array (FPGA) with a custom firmware.

The waveguides are characterized at a nominal temperature of 4 K (4K) using the pulse tube cooler of a cryogen-free dilution refrigerator system in which also the millikelvin temperature (BT) measurements are performed. We thermally anchor the waveguides to the base plate of the cryostat using OFHC copper braids and clamps. The actual waveguide temperatures are extracted in a measurement of the resistance of a calibrated ruthenium oxide (RuO) sensor mounted at the center of the coaxial cables or at the end of the rectangular waveguides and are listed in Table 1.

For the measurements at base temperature BT (~ 10 mK) it proved essential to carefully anchor all superconducting waveguide elements at multiple points to assure best possible thermalization. The measured temperatures listed in Table 1 are found to be significantly higher than the BT specified above. We attribute the incomplete thermalization of the superconducting waveguides to the small thermal conductivity of the employed materials below their critical temperature T_c [36]. We note that when using only a minimal set of anchoring points, we observed even higher temperatures.

3 Measurements of the attenuation constant

3.1 Illustration of the measurement technique

To illustrate the resonant-cavity technique for extracting the attenuation constant of a waveguide we discuss a calibrated S-parameter measurement at RT for the coaxial line CC141A1 (Table 1). The measured transmission spectrum $|S_{21}(\nu)|^2$ exemplifies the periodic structure of higher-order modes for mode numbers n between 5 and 109 (Figure 2). We extract the resonance frequency ν_n and the external and internal quality factor, Q_e and Q_i , for each mode n by fitting the complex transmission coefficient of a weakly coupled parallel RLC circuit (see Appendix 2) to the data in a finite bandwidth around each ν_n (Figure 3). We observe a decreasing insertion loss on resonance $IL(\nu_n) = -10 \log_{10} |S_{21}(\nu_n)|^2$ dB (dashed line in Figure 2(a)) with increasing frequency due to the increase of the effective capacitive coupling strength. We chose $IL(\nu_n) > 40$ dB to ensure the largely undercoupled regime ($Q_e \gg Q_i$) over the entire frequency range. In this regime, Q_i is well approximated by the loaded quality factor Q_l according to $1/Q_l = 1/Q_i - 1/Q_e \approx 1/Q_i$. In our experiments we assure that $Q_e > 10Q_i$ for all frequencies and temperatures.

Under this condition it is sufficient to extract Q_l for each mode n from

$$|S_{21}(\nu)| = \frac{S_n^{\max}}{\sqrt{1 + 4(\nu/\nu_n - 1)^2 Q_l^2}} + C_1 + C_2 \nu \quad (1)$$

neglecting the specific value of the insertion loss (S_n^{\max} is a free scaling factor). C_1 , C_2 account for a constant offset and a linear frequency dependence in the background [37] most relevant for measurements of low quality factors ($< 10^3$) resonances.

3.2 Analysis of coaxial lines

To determine the frequency dependence of the attenuation constant $\alpha(\nu)$ of the coaxial line we analyze its measured quality factors Q_l in dependence on the mode number n . The

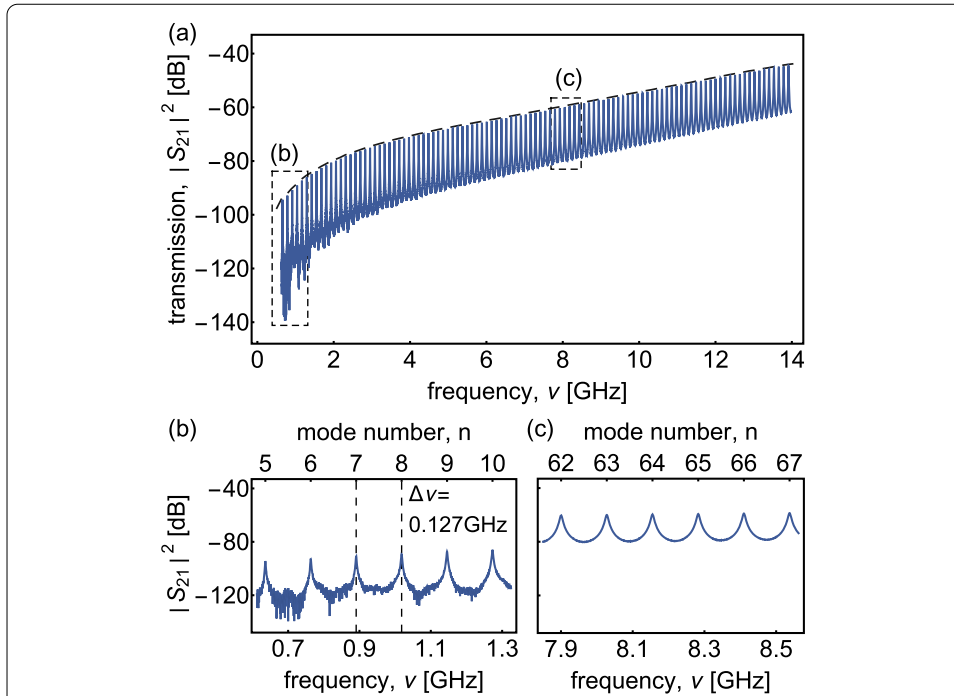


Figure 2 Exemplary waveguide resonator transmission spectra at room temperature. (a) Transmission coefficient $|S_{21}|^2$ versus frequency ν for CC141Al at RT. The dashed line indicates the frequency-dependent insertion loss on resonance $IL(\nu_n)$. $|S_{21}|^2$ of (b) the first 6 measured modes and (c) 6 modes around 8 GHz as indicated by the dashed boxes in (a).

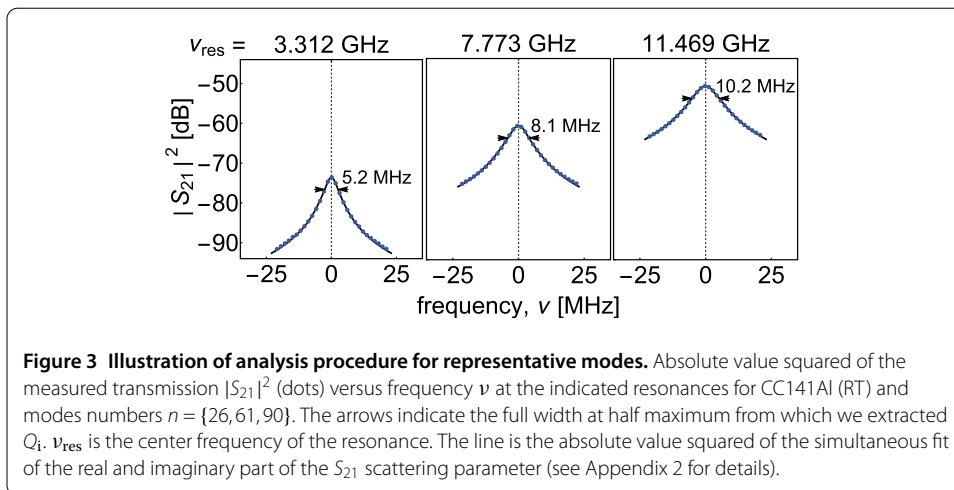


Figure 3 Illustration of analysis procedure for representative modes. Absolute value squared of the measured transmission $|S_{21}|^2$ (dots) versus frequency ν at the indicated resonances for CC141Al (RT) and modes numbers $n = \{26, 61, 90\}$. The arrows indicate the full width at half maximum from which we extracted Q_i . ν_{res} is the center frequency of the resonance. The line is the absolute value squared of the simultaneous fit of the real and imaginary part of the S_{21} scattering parameter (see Appendix 2 for details).

fundamental frequency ν_0 of a low-loss transmission line resonator is given by

$$\nu_0 = \frac{c}{\sqrt{\epsilon_r}} \frac{1}{2l} \tag{2}$$

with the length of the resonator l , the relative permittivity of the dielectric ϵ_r and the speed of light in vacuum c . The internal quality factor Q_i [38]

$$Q_i = \frac{n\pi}{2l\alpha} \tag{3}$$

is inversely proportional to α

$$\alpha = \alpha_c + \alpha_d = \frac{g_c \sqrt{\epsilon_r}}{2\mu_0 c} R_s(\nu) + \frac{\pi \sqrt{\epsilon_r}}{c} \nu \tan \delta. \quad (4)$$

α can be written as a sum of conductor loss α_c and dielectric loss α_d with the vacuum permeability μ_0 , a frequency dependent surface resistance $R_s(\nu)$, a geometric constant g_c and the frequency independent loss tangent of the dielectric material $\tan \delta$. For a coaxial line g_c is $(1/a + 1/b)/\ln(b/a)$ with the radius of the center conductor a and the inner radius of the outer conductor b . To characterize the conductor loss of coaxial cables combining different materials for the center and outer conductors we introduce an effective surface resistance R_s (see Appendix 3). Inserting Eq. (4) into Eq. (3) leads to

$$Q_i(\nu_n) = \frac{1}{\frac{g_c}{2\pi\mu_0} \frac{R_s(\nu_n)}{\nu_n} + \tan \delta}, \quad (5)$$

which is independent of ϵ_r . Therefore, ϵ_r is extracted from the fundamental frequency of the resonator ν_0 and $R_s(\nu)$ and $\tan \delta$ from measurements of $Q_i(\nu)$.

The surface resistance of a normal conductor $R_s^{\text{nc}}(\nu)$ is proportional to $\sqrt{\nu}$ and to the direct current (dc) conductivity $1/\sqrt{\sigma}$ [38]. The theory of the high-frequency dissipation in superconductors [39–42] shows a quadratic dependence of $R_s^{\text{sc}}(\nu)$.

The measured external quality factors at RT (Figure 4(b) and Figure 5(b)) are in good agreement with the ones expected for a capacitively coupled transmission line [43]

$$Q_e(\nu_n) = \frac{C_l l}{8\pi C_c^2 R_l} \frac{1}{\nu_n} + \frac{R_l C_l l \pi}{2} \nu_n, \quad (6)$$

with the capacitance per unit length C_l , the real part of the load impedance R_l and the coupling capacitance C_c used as fit parameters. An interpolation of the Q_e measurements is used in the 4K and BT measurements to estimate the average number of photons stored in the waveguide on resonance at each mode n (Table 1).

The frequency dependence of the measured quality factors for CC141Al presented in Figure 4(a) shows the expected $\sqrt{\nu}$ dependence considering an effective conductivity of the outer and center conductor following the skin effect model of normal conductor. This suggests that α_c is mainly limited by the normal conducting SPC center conductor. The dielectric loss limit of Q_i is determined to be approximately 15×10^3 at BT, see Table 2.

Following the same measurement procedure, we extract the quality factor of low-loss superconducting cables (e.g. see Figure 5 for CC085NbTi). The measured internal quality factors of CC085NbTi at the 4K and BT, ranging from 12×10^3 to 92×10^3 , decrease approximately $\propto \nu^2$ (solid line) with a small deviation at higher frequencies. We obtain a better fit assuming a power law dependence of $R_s^{\text{sc}}(\nu) \propto \nu^p$ with an exponent $p \approx 2.7 \pm 0.3$ at 4K and $p \approx 3.4 \pm 0.5$ at BT. This peculiar frequency dependence is not explained by the theory of high-frequency dissipation in superconductors [39–42]. Measuring CC085Nb leads to similar results as for CC085NbTi (Figure 6). We also observe a power law dependence with $p \approx 3.2 \pm 0.4$ and $p \approx 3.3 \pm 0.3$ at 4K and BT. Furthermore, we compare the dielectric and conductor properties of these low-loss coaxial cables with those of CC085Cu for which we measured attenuation ranging from 0.30 dB/m to 0.75 dB/m (Figure 6). In addition, we measured the attenuation constant of a stainless steel outer and center

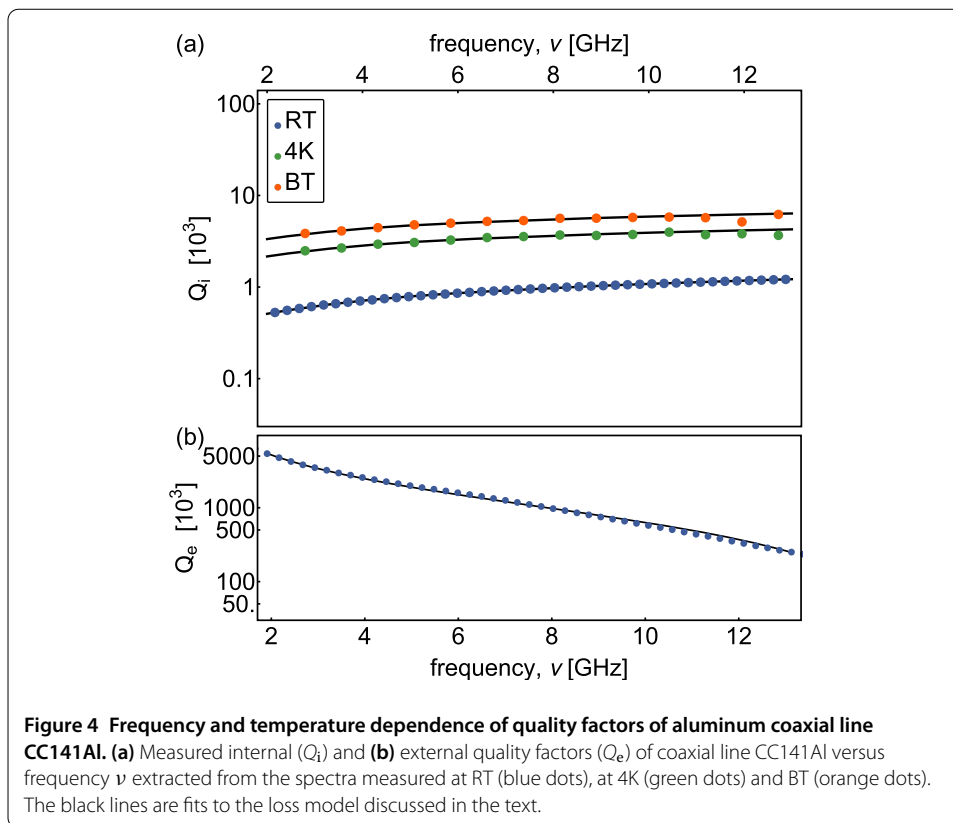


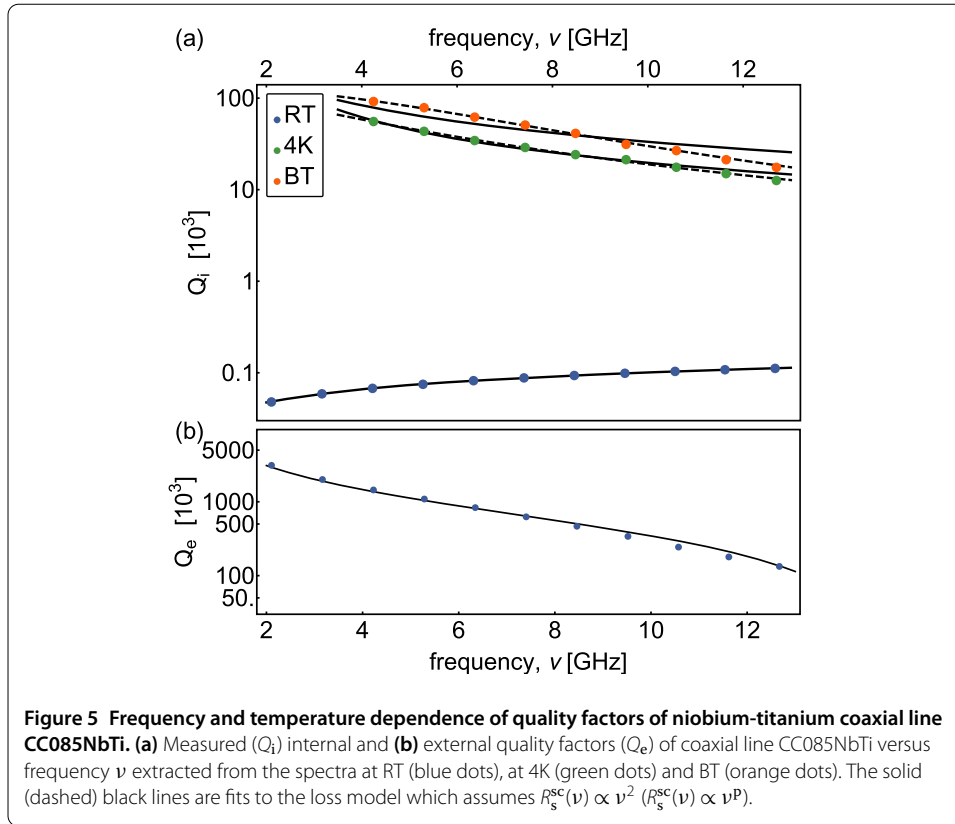
Table 2 Summary of the extracted relative permittivities ϵ_r and loss tangents $\tan \delta$ of the tested dielectric materials

T/parameter	Micro-Coax LD PTFE	Keycom ldPTFE	Micro-Coax sPTFE
ϵ_r			
RT	1.70 ± 0.01	1.72 ± 0.06	1.98 ± 0.07
4K	1.70 ± 0.01	1.72 ± 0.06	2.01 ± 0.07
BT	1.70 ± 0.01	1.72 ± 0.06	2.01 ± 0.07
$\tan \delta [\times 10^{-5}]$			
RT	9 ± 1		25 ± 4
4K	8.5 ± 0.2	0.8 ± 0.2	22 ± 2
BT	6.6 ± 0.2	0.7 ± 0.1	19 ± 4

The methods used for the extraction of these parameters are discussed in the text.

conductor coaxial cable (CC085SS) at RT, approximately 77 K (LN2) and 4.2 K (LHe) described in Appendix 4.

We extract the relative permittivities ϵ_r from Eq. (2) and the loss tangent $\tan \delta$ from fitting Eq. (5) to the measured $Q_i(\nu)$ for each coaxial cable (Table 2). The values for the Micro-Coax ldPTFE are determined from CC141Al measurements, for the Micro-Coax sPTFE from CC085Cu and for the Keycom ldPTFE from CC085NbTi and CC085Nb measurements. We extract $\tan \delta$ of the Keycom ldPTFE from the fit assuming $R_s^{sc}(\nu) \propto \nu^p$ at 4K and BT. Due to the low internal quality factors $Q_i < 100$ limited by the low RT conductivity (measured $\sigma \approx 8 \times 10^5$ S/m for NbTi and Nb) we are unable to extract these quantities at RT. At cryogenic temperature we observe that $\tan \delta$ of the ldPTFE of Micro-Coax and



Keycom differ by a factor of ~ 10 . ϵ_r is found to be ~ 1.7 for ldPTFE and ~ 2 for sPTFE and is nearly temperature independent.

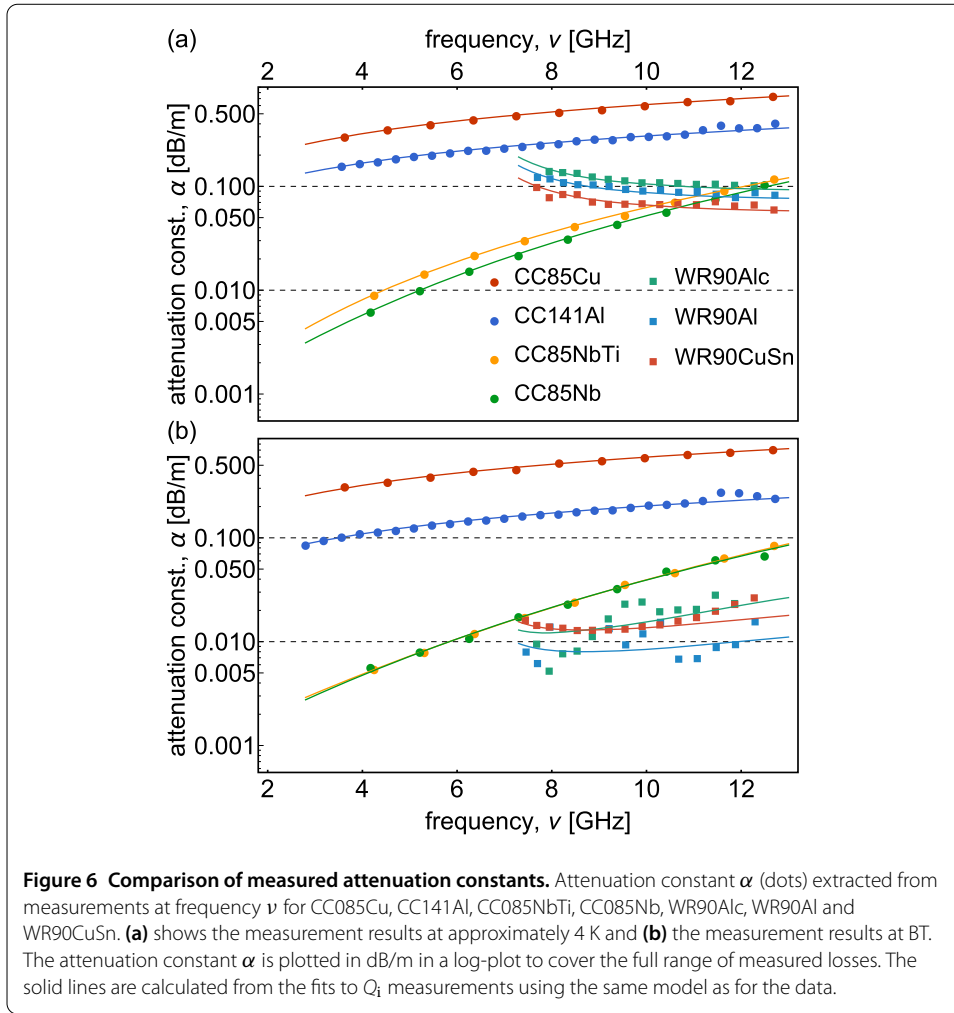
3.3 Analysis of rectangular waveguides

We performed similar measurements with three different rectangular waveguides of type WR90 (see Table 1). We use an aperture coupling approach by installing two aluminum 1100 plates (thickness $t_a = 3$ mm) at both ends with a circular aperture (radius $r_a = 5.3$ mm for WR90Alc and $r_a = 4.1$ mm for WR90Al and WR90CuSn) in the center (Figure 1) resulting in inductively coupled rectangular 3D cavities [44]. The coupling strength depends on r_a and t_a of the aperture plates. We perform finite element simulation to estimate the coupling (for details see Appendix 1) and determine the attenuation constant of the rectangular waveguides by a measurement of its internal quality factor. For rectangular waveguide cavities the frequencies of the transverse electric modes TE_{10k} are given by

$$\nu_k = \frac{c}{2} \sqrt{\frac{1}{s_1^2} + \frac{k^2}{l^2}} \tag{7}$$

with length of the longer transverse dimension of the rectangular waveguide s_1 and the length of the cavity l . The frequency dependent internal quality factor is [38]

$$Q_{TE_{10k}}(\nu_k) = \frac{2s_1^3 s_2 l \pi \mu_0 \nu_k^3}{R_s(\nu_k) c^2 s_2 (l - s_1) + 2s_1^3 (2s_2 + l) \nu_k^2} \tag{8}$$



with the length of the shorter transverse dimension of the rectangular waveguide s_2 . Inverting Eq. (8) we extract the surface resistance $R_s(\nu_k)$ from a measurement of $Q_{TE_{10k}}(\nu_k)$ which we use to calculate the attenuation constant of the TE_{10} mode of a rectangular waveguide

$$\alpha_{TE_{10}}(\nu) = \frac{R_s(\nu)}{s_1^2 s_2 \mu_0 c} \frac{s_2 c^2 + 2s_1^3 \nu^2}{\nu \sqrt{4\nu^2 s_1^2 - c^2}}. \tag{9}$$

Using this model we extract the attenuation constant of the rectangular waveguides, ranging from 0.06 dB/m to 0.17 dB/m at 4K and 0.007 dB/m to 0.02 dB/m at BT, and determine the frequency dependence of the internal quality factor. For the rectangular waveguides in the normal state at 4K we find good agreement to the theoretical model by considering the normal state surface resistance $R_s^{nc}(\nu) \propto \sqrt{\nu}$. At BT in the superconducting state a surface resistance $R_s^{sc}(\nu) \propto \nu^2$ approximates the data (Figure 6). Note that, the frequency dependence cannot be extracted with high accuracy for superconducting rectangular waveguides, since $\alpha_{TE_{10}}(\nu)$ diverges towards the cutoff frequency $\nu_{co} = c/2s_1$.

4 Conclusions

We have presented measurements of the attenuation constant of commonly used, commercially available low-loss coaxial cables and rectangular waveguides down to millikelvin temperatures in a frequency range between 3.5 and 12.8 GHz. We have performed measurements of attenuations constants down to 0.005 dB/m using a resonant-cavity technique at cryogenic temperatures. In this method, we employ weak couplings to the waveguides resulting in resonant standing waves and measure their quality factors. We have extracted the loss tangent and relative permittivity of different dielectric materials by comparing our measurement results to existing loss models. The frequency dependence of the internal quality factors of the normal conducting waveguides are well described by the loss model, while the tested CC085NbTi and CC085Nb show small deviations from the predictions for the high-frequency dissipation in superconductors [39, 40]. We have also studied the power dependence of the attenuation constant which we find to be independent of the input power in a range from -140 to -80 dBm (see Appendix 5).

Our results indicate that transmitting signals on a single photon level is feasible within laboratory distances, e.g. 95% of the signal can be transmitted over distances of 28 m using commercial rectangular waveguides or 8 m using coaxial cables. Furthermore, we find no significant dependence of the attenuation constants on the ambient residual magnetic fields in measurements performed with and without cryoperm magnetic shielding (see Appendix 6).

Comparing our results to recent measurements of high quality 3D cavities [45] with quality factors up to 7×10^7 indicate that improving the surface treatment of rectangular waveguides may lead to a even lower attenuation constant of rectangular waveguides down to $\sim 10^{-4}$ dB/m. Furthermore, our measurements show that the loss tangent $\tan \delta$ strongly depends on the PTFE composite where $\tan \delta \sim 2 \times 10^{-6}$ of PTFE have been reported at cryogenic temperatures [46, 47] about a factor of 4 lower than those measured here. This suggests that the loss of superconducting coaxial cables may also be further reduced.

Appendix 1: Characterization of the input/output coupling

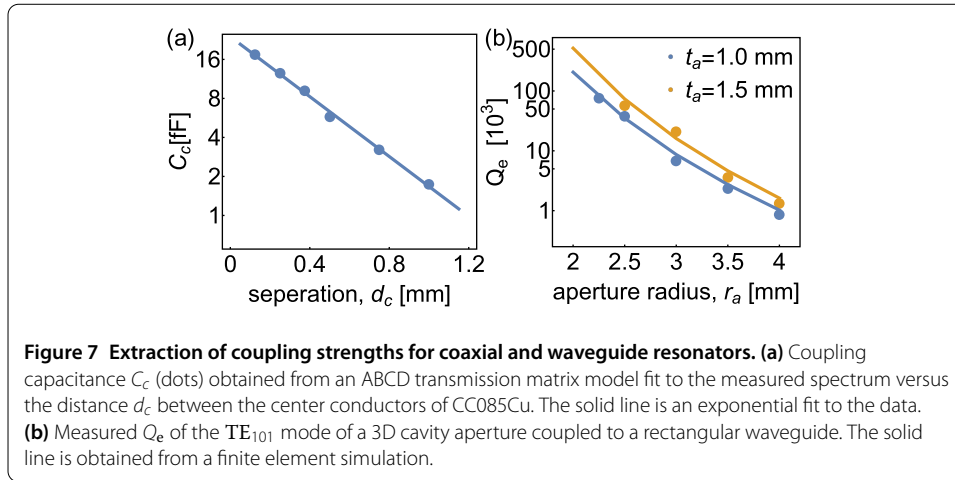
We extract the coupling capacitance C_c between the input coupler and the center conductor of the coaxial line CC085Cu from a fit of the measured transmission spectrum to an ABCD transmission matrix model. We find C_c to decrease exponentially with the separation d_c , see Figure 1 and solid line in Figure 7(a).

We determine the external quality factor Q_e of an aperture coupled 3D cavity with resonance frequency $\nu_{101} = 8.690$ GHz in dependence on the coupling wall thickness t_a and the radius of the circular aperture r_a (Figure 1). We find good agreement between the measured Q_e and the one extracted from finite-element simulations [48], Figure 7(b).

By changing the geometry of the described couplers, the coupling of both coaxial cables and rectangular waveguides can be tuned by orders of magnitude which is sufficient to fulfill the condition $Q_e \gg Q_i$ to extract Q_i precisely.

Appendix 2: Weakly coupled parallel RLC circuit

To extract the resonance frequency ν_n and the external and internal quality factor, Q_e and Q_i , of the investigated devices we simultaneously fit the real and imaginary part of the



complex transmission coefficient

$$S_{21}(v) = \left(\frac{1}{1 + Q_e/Q_i + 2iQ_e(v/v_n - 1)} + X \right) e^{i\phi} \quad (10)$$

of a weakly coupled parallel RLC circuit [37]. Here X is a complex constant which accounts for impedance mismatches in the SMA panel mount connectors and $e^{i\phi}$ is a rotation of the data relative to the measurement plane [49, 50].

Appendix 3: Attenuation constant of low-loss coaxial cables

We state the derivation of the attenuation constant of a low-loss transmission line based on Ref. [38]. The equivalent circuit parameters (self-inductance per unit length L_1 , capacitance per unit length C_1 , series resistance per unit length R_1 and shunt conductance per unit length G_1) can be derived from the electric and magnetic field of the transmission line

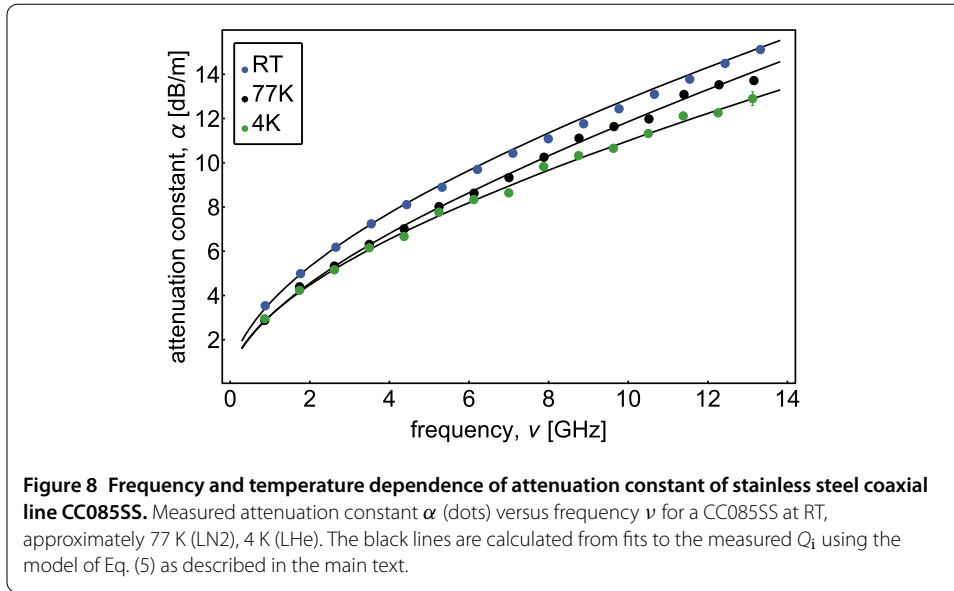
$$\begin{aligned} L_1 &= \frac{\mu}{2\pi} \ln b/a, \\ C_1 &= \frac{2\pi\epsilon_0\epsilon_r}{\ln b/a}, \\ R_1 &= \frac{1}{2\pi} \left(\frac{R_s^a}{a} + \frac{R_s^b}{b} \right), \\ G_1 &= \frac{2\pi\omega\epsilon_0\epsilon_r \tan \delta}{\ln b/a}. \end{aligned} \quad (11)$$

The complex propagation constant

$$\gamma = \alpha + i\beta = \sqrt{(R_1 + i\omega L_1)(G_1 + i\omega C_1)} \quad (12)$$

can be approximated for small conductor $R_1 \ll \omega L_1$ and dielectric loss $G_1 \ll \omega C_1$ by

$$\gamma \approx i\omega\sqrt{L_1 C_1} \left(1 - \frac{i}{2} \left(\frac{R_1}{Z_0} + G_1 Z_0 \right) \right) \quad (13)$$



with the characteristic impedance of the line $Z_0 = \sqrt{L_1/C_1}$, so that

$$\beta = \omega\sqrt{L_1C_1} = \frac{\omega\sqrt{\epsilon_r}}{c}, \tag{14}$$

$$\begin{aligned} \alpha &= \frac{1}{2} \left(\frac{R_1}{Z_0} + G_1Z_0 \right) \\ &= \frac{\sqrt{\epsilon_r}}{2c \ln b/a} \left(\frac{R_s^a}{a} + \frac{R_s^b}{b} \right) + \frac{\pi\nu\sqrt{\epsilon_r}}{c} \tan \delta \\ &= \frac{R_s\sqrt{\epsilon_r}}{2c \ln b/a} \left(\frac{1}{a} + \frac{1}{b} \right) + \frac{\pi\nu\sqrt{\epsilon_r}}{c} \tan \delta. \end{aligned} \tag{15}$$

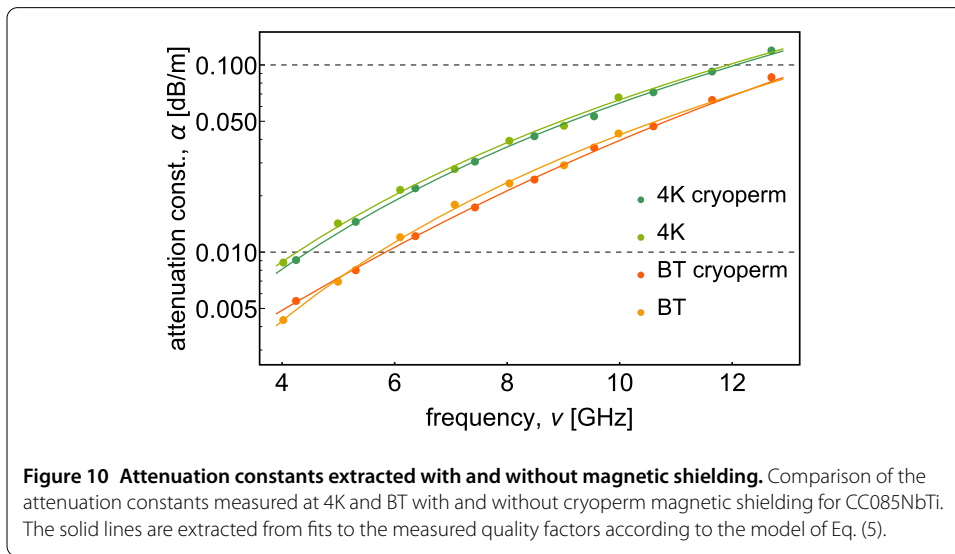
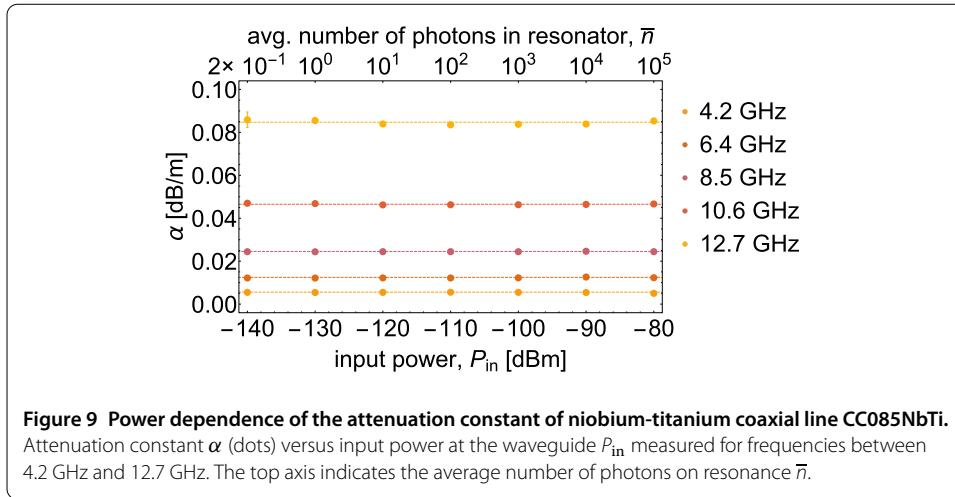
In the last step we introduced an effective surface resistance $R_s = R_s^a = R_s^b$ to characterize the conductor loss. This is necessary, since we cannot distinguish the contributions of the different materials of the center and outer conductors to the total conductor loss in our data.

Appendix 4: Attenuation constant of CC085SS

We evaluate the loss of a 2.2 mm (0.085 in) diameter stainless steel outer and center conductor coaxial cable (CC085SS) typically used in cryogenic applications where loss is of little concern, i.e. in input drive lines. At RT, approximately 77 K (LN2) and 4.2 K (LHe), the cable manufactured by Micro-Coax, Inc. [33] shows the expected frequency dependent attenuation $\propto \sqrt{\nu}$ of a normal conductor decreasing with temperature (Figure 8). For example, we extract attenuation constants at 6 GHz of 9.7 dBm/m (RT), 8.7 dBm/m (LN2) and 8.2 dBm/m (LHe).

Appendix 5: Power dependence of the attenuation constant

We find the measured attenuation constant of CC085NbTi to be independent of the input power in a range from -140 to -80 dBm corresponding to an average photon number on



resonance inside the resonator of 10^5 to 0.2 and an average resonator voltage $\langle V^2 \rangle^{1/2}$ of approximately 10^{-6} to 10^{-4} V (Figure 9). Our voltage range is comparable to that of Ref. [51] in which a clear power dependence for SiO_2 and SiN_x dielectric materials is observed and explained by the loss due to the coupling of microscopic two level systems (TLS) to the electromagnetic field within the resonator [52]

$$\delta_{\text{TLS}}(P_r) = \frac{\delta_{\text{TLS}}^0}{\sqrt{1 + P_r/P_c}} \tag{16}$$

with the low power TLS loss δ_{TLS}^0 and a characteristic power P_c depending on the dielectric material. Following this model we conclude that the field inside the dielectric material of the coaxial cable (ldPTFE) does not saturate the individual TLS in the measured power range [53, 54], since no power dependence of the attenuation of the coaxial cable is observed.

Appendix 6: Dependence on ambient magnetic field

We compare the extracted attenuation constants of CC085NbTi cables within (length 110 mm) and without (length 810 mm) a cryoperm magnetic shield and find no significant effect at 4K and BT (Figure 10). Since we expect the internal loss to be the sum of the individual loss contributions we argue that the measured attenuation constants are not limited by an ambient magnetic field which is believed to be dominated by the isolators installed at the BT stage of the used dilution refrigerator system.

Competing interests

The authors declare that they have no competing interests.

Authors' contributions

The design of the experiment was developed by PK and AW. The experiments were performed by PK, TW and PM. The data was analyzed and interpreted by PK, TW and YS. The FPGA firmware was implemented and its operation overseen by YS. The manuscript was written by PK and AW. All authors commented on the manuscript. The project was led by AW. All authors have read and approved the final manuscript.

Acknowledgements

The authors thank Tobias Frey, Silvia Ruffieux and Maud Barthélemy for their contributions to the measurements, Oscar Akerlund for his support with the numerical integration, Christopher Eichler for discussing the manuscript and Keycom Corporation for providing superconducting coaxial cables. This work is supported by the European Research Council (ERC) through the "Superconducting Quantum Networks" (SuperQuNet) project, by National Centre of Competence in Research "Quantum Science and Technology" (NCCR QSIT), a research instrument of the Swiss National Science Foundation (SNSF), by the Office of the Director of National Intelligence (ODNI), Intelligence Advanced Research Projects Activity (IARPA), via the U.S. Army Research Office grant W911NF-16-1-0071 and by ETH Zurich. The views and conclusions contained herein are those of the authors and should not be interpreted as necessarily representing the official policies or endorsements, either expressed or implied, of the ODNI, IARPA, or the U.S. Government. The U.S. Government is authorized to reproduce and distribute reprints for Governmental purposes notwithstanding any copyright annotation thereon.

Endnotes

- ^a Per the standard specification for silver-coated soft or annealed copper wire (ASTM B-298).
^b Per the standard specification for silver-coated, copper-clad steel wire (ASTM B-501).

Publisher's Note

Springer Nature remains neutral with regard to jurisdictional claims in published maps and institutional affiliations.

Received: 2 March 2017 Accepted: 4 April 2017 Published online: 04 May 2017

References

- DiVincenzo DP. *Fortschr Phys.* 2000;48:771.
- Petta JR, Johnson AC, Taylor JM, Laird EA, Yacoby A, Lukin MD, Marcus CM, Hanson MP, Gossard AC. *Science.* 2005;309:2180.
- Frey T, Leek PJ, Beck M, Blais A, Ihn T, Ensslin K, Wallraff A. *Phys Rev Lett.* 2012;108:046807.
- Maune BM, Borselli MG, Huang B, Ladd TD, Deelman PW, Holabird KS, Kiselev AA, Alvarado-Rodriguez I, Ross RS, Schmitz AE, Sokolich M, Watson CA, Gyure MF, Hunter AT. *Nature.* 2012;481:344.
- Delbecq MR, Schmitt V, Parmentier FD, Roch N, Viennot JJ, Fève G, Huard B, Mora C, Cottet A, Kontos T. *Phys Rev Lett.* 2011;107:256804.
- Pla JJ, Tan KY, Dehollain JP, Lim WH, Morton JLL, Jamieson DN, Dzurak AS, Morello A. *Nature.* 2012;489:541.
- Kubo Y, Ong FR, Bertet P, Vion D, Jacques V, Zheng D, Dréau A, Roch J-F, Auffeves A, Jelezko F, Wrachtrup J, Barthe MF, Bergonzo P, Esteve D. *Phys Rev Lett.* 2010;105:140502.
- Chiorescu I, Bertet P, Semba K, Nakamura Y, Harmans CJPM, Mooij JE. *Nature.* 2004;431:159.
- Wallraff A, Schuster DI, Blais A, Frunzio L, Huang R-S, Majer J, Kumar S, Girvin SM, Schoelkopf RJ. *Nature.* 2004;431:162.
- Devoret M, Schoelkopf RJ. *Science.* 2013;339:1169.
- Hagley E, Maitra X, Nogues G, Wunderlich C, Brune M, Raimond JM, Haroche S. *Phys Rev Lett.* 1997;79:1.
- Raimond JM, Brune M, Haroche S. *Rev Mod Phys.* 2001;73:565.
- Haroche S, Raimond J-M. *Exploring the quantum: atoms, cavities, and photons.* New York: Oxford University Press; 2006.
- Hogan SD, Agner JA, Merkt F, Thiele T, Filipp S, Wallraff A. *Phys Rev Lett.* 2012;108:063004.
- Eichler C, Bozyigit D, Lang C, Steffen L, Fink J, Wallraff A. *Phys Rev Lett.* 2011;106:220503.
- Eichler C, Lang C, Fink JM, Govenius J, Filipp S, Wallraff A. *Phys Rev Lett.* 2012;109:240501.
- Roch N, Schwartz ME, Motzoi F, Macklin C, Vijay R, Eddins AW, Korotkov AN, Whaley KB, Sarovar M, Siddiqi I. *Phys Rev Lett.* 2014;112:170501.
- Narla A, Shankar S, Hatridge M, Leghtas Z, Sliwa KM, Zalys-Geller E, Mundhada SO, Pfaff W, Frunzio L, Schoelkopf RJ, Devoret MH. *Phys Rev X.* 2016;6:031036.
- Cirac JI, Zoller P, Kimble HJ, Mabuchi H. *Phys Rev Lett.* 1997;78:3221.

20. Pechal M, Huthmacher L, Eichler C, Zeytinoglu S, Abdumalikov A Jr., Berger S, Wallraff A, Filipp S. *Phys Rev X*. 2014;4:041010.
21. Zeytinoglu S, Pechal M, Berger S, Abdumalikov AA Jr., Wallraff A, Filipp S. *Phys Rev A*. 2015;91:043846.
22. Wenner J, Yin Y, Chen Y, Barends R, Chiaro B, Jeffrey E, Kelly J, Megrant A, Mutus J, Neill C, O'Malley P, Roushan P, Sank D, Vainsencher A, White T, Korotkov AN, Cleland A, Martinis JM. *Phys Rev Lett*. 2014;112:210501.
23. Macklin C, O'Brien K, Hover D, Schwartz ME, Bolkhovskiy V, Zhang X, Oliver WD, Siddiqi I. *Science*. 2015;350:307. <http://www.sciencemag.org/content/350/6258/307.full.pdf>.
24. McCaa WD, Nahman NS. *J Appl Phys*. 1969;40:2098.
25. Ekstrom MP, McCaa WD, Nahman NS. *IEEE Trans Nucl Sci*. 1971;18:18.
26. Chiba N, Kashiwayanagi Y, Mikoshiba K. *Proc IEEE*. 1973;61:124.
27. Giordano S, Hahn H, Halama H, Luhman T, Bauer W. *IEEE Trans Magn*. 1975;11:437.
28. Mazuer J. *Cryogenics*. 1978;18:39.
29. Peterson GE, Stawicki RP. *J Am Ceram Soc*. 1989;72:704.
30. Kushino A, Kasai S, Kohjiro S, Shiki S, Ohkubo M. *J Low Temp Phys*. 2008;151:650.
31. Kushino A, Teranishi Y, Kasai S. *J Supercond Nov Magn*. 2013;26:2085.
32. Keycom characteristic technologies. 2016. Accessed: 2016-05-18.
33. Cable manufacturers, cable assemblies - micro-coax, inc. 2016. Accessed: 2016-05-18
34. Penn engineering components: waveguide specialists. 2016. Accessed: 2016-05-18
35. Lang C. Quantum microwave radiation and its interference characterized by correlation function measurements in circuit quantum electrodynamics [Ph.D. thesis]. Zurich: ETH; 2014.
36. Pobell F. *Matter and methods at low temperatures*. 3rd ed. Berlin: Springer; 2006.
37. Petersan PJ, Anlage SM. *J Appl Phys*. 1998;84:3392.
38. Pozar DM. *Microwave engineering*. Hoboken: Wiley; 2012.
39. Tinkham M. *Introduction to superconductivity*. 2nd ed. Mineola: Dover; 2004.
40. Mattis DC, Bardeen J. *Phys Rev*. 1958;111:412.
41. Kose V. *Superconducting quantum electronics*. Berlin: Springer; 1989.
42. Gao J. *The physics of superconducting microwave resonators* [Ph.D. thesis]. California Institute of Technology; 2008.
43. Göppl M, Fragner A, Baur M, Bianchetti R, Filipp S, Fink JM, Leek PJ, Puebla G, Steffen L, Wallraff A. *J Appl Phys*. 2008;104:113904.
44. Collin R. *Field theory of guided waves*. New York: IEEE Press; 1991.
45. Reagor M, Paik H, Catelani G, Sun L, Axline C, Holland E, Pop IM, Masluk NA, Brecht T, Frunzio L, Devoret MH, Glazman LI, Schoelkopf RJ. *Appl Phys Lett*. 2013;102:192604.
46. Geyer RG, Krupka J. *IEEE Trans Instrum Meas*. 1995;44:329.
47. Jacob MV, Mazierska J, Leong K, Krupka J. *IEEE Trans Microw Theory Tech*. 2002;50:474.
48. COMSOL4.3. *Comsol multiphysics® v. 4.3*, 2012.
49. Leong K, Mazierska J. *IEEE Trans Microw Theory Tech*. 2002;50:2115.
50. Probst S, Song FB, Bushev PA, Ustinov AV, Weides M. *Rev Sci Instrum*. 2015;86:024706.
51. Martinis JM, Cooper KB, McDermott R, Steffen M, Ansmann M, Osborn KD, Cicak K, Oh S, Pappas DP, Simmonds RW, Yu CC. *Phys Rev Lett*. 2005;95:210503.
52. Goetz J, Deppe F, Haerberlein M, Wulschner F, Zollitsch CW, Meier S, Fischer M, Eder P, Xie E, Fedorov KG, Menzel EP, Marx A, Gross R. *J Appl Phys*. 2016;119:015304. doi:10.1063/1.4939299.
53. Von Schickfus M, Hunklinger S. *Phys Lett A*. 1977;64:144.
54. Lindström T, Healey JE, Colclough MS, Muirhead CM, Tzalenchuk AY. *Phys Rev B*. 2009;80:132501.

Submit your manuscript to a SpringerOpen[®] journal and benefit from:

- Convenient online submission
- Rigorous peer review
- Immediate publication on acceptance
- Open access: articles freely available online
- High visibility within the field
- Retaining the copyright to your article

Submit your next manuscript at ► springeropen.com
